A Generalized Pore Model for Gas-Solid Reactions Exhibiting Pore Closure

A model of pore structure evolution has been developed for gas-solid reactions exhibiting pore closure behavior. A cylindrical pore network of constant coordination number is used to represent the porous medium, and both discrete and continuous distributions of pore size are considered. The mathematical model takes into consideration the effects of pore overlapping and nonuniform pore growth, and follows the formation of inaccessible volume in the interior of the reacting particles by use of percolation theory concepts. The model is applied, along with an appropriate diffusion and reaction model, to the investigation of the transient behavior of calcined limestone particles in an environment of sulfur dioxide.

Huei-Chung Yu, S. V. Sotirchos
Department of Chemical Engineering
University of Rochester
Rochester, NY 14627

Introduction

Noncatalytic gas-solid reactions with solid product are encountered in a number of chemical process industries. Important applications include the use of limestone to control SO_2 emissions from fluidized-bed combustors and the use of metal oxides in coal gas desulfurization processes. Because of the formation of the solid product, a number of processes must be considered in the development of single-particle models for the above gas-solid systems, in addition to intraparticle diffusion and reaction. The structure of the reacting solid, for instance, is described by two temporally and spatially evolving surfaces, the reaction surface (solid reactant-solid product interface) and the pore surface. Because of the slow diffusion of reactive species in the product layer, large concentration gradients may be present in the product layer even if appreciable concentration gradients do not exist in the porous structure.

The presence of the solid product may lead to additional complications if the stoichiometric volume ratio of the system, i.e., the ratio of the molar volume of solid product to stoichiometrically equivalent volume of solid reactant, Z, is greater than one. Since the solid product occupies more space than the solid from which it has resulted, the porosity diminishes with the progress of the reaction and incomplete conversion and pore plugging phenomena might be observed. Such behavior is experimentally observed in a number of gas-solid systems, such as in the CaO-SO_2 system (Hartman and Coughlin, 1976) and in the hydrofluorination of UO_2 (Costa and Smith, 1971). Under conditions of significant concentration gradients in the interior of the reacting particles, pore closure may first occur at the external surface, preventing further penetration of the reactive gases and subsequent reaction in the interior. Another phenomenon that may take place in gas-solid noncatalytic systems exhibiting pore closure behavior is the formation of inaccessible pore space. This situation results when the feeder pores of a finite cluster of pores are filled with solid product.

Structural models that model the void space of a reacting solid by a population of pores are frequently used in gas-solid reactions. Most pore models presented in the past employ assumptions of uniform pore size and negligible pore overlap. However, the overlapping of adjacent pores becomes significant as the conversion increases, and most porous solids are characterized by distributed pore size. Different size pores close at different times if pore closure occurs—the smaller the pores, the earlier they close—and hence different reactivity evolution patterns may be observed for solids with the same initial porosity and surface area.

Random-pore models for solids with a pore size distribution, with or without pore closure, were recently presented by Sotirchos and Yu (1984, 1985) for use under reaction conditions controlled by intrinsic kinetics and diffusion in the product layer. The models can be used for any type of pore size distribution and take into account the effects of pore overlap on the diffusion flux in the product layer and on the evolution of the reaction and pore surfaces. A similar structural model was also developed by Bhatia (1985). A simplified version of the general model was developed by Sotirchos and Yu (1985) to be used in cases where the differences in the growth rates of pores of different curvature

Correspondence concerning this paper should be addressed to S. V. Sotirchos.

are small. It is interesting to point out that the simplified model is practically described by a single ordinary differential equation, and hence the numerical effort involved in its solution is comparable to or even less than that of structural models developed in the past for uniformly sized pore systems.

The above structural models consider an initial pore structure visualized as a random assembly of infinitely long, cylindrical capillaries. The real porous network, on the other hand, most probably consists of interconnected pores of varying cross section along their length. For gas-solid systems with pore closure behavior ($Z > 1$), the narrow-neck regions will close first, as the reaction progresses, causing the formation of inaccessible pore space in the interior. This, however, is precluded by the infinitely long pores used in the random-pore models. The formation of inaccessible pore volume may be described by employing percolation theory concepts, as Yortsos and Sharma (1984) did in a structural model they developed. Like most structural models, however, their model is valid only over a limited conversion range, since it does not consider pore overlapping with the extent of the reaction. In addition, the model was developed for networks of parallel-plate geometry pores, and consequently it does not apply to pore systems exhibiting nonuniform pore growth.

General structural models that take into account almost all phenomena met in gas-solid reactions with solid product are developed in the present study. Networks of cylindrical capillaries, distributed both in size and length, are used to described the evolving reaction and pore surfaces. Using percolation theory in a manner similar to that of Yortsos and Sharma (1984), the formation of inaccessible pore volume is followed with the extent of the reaction. Our structural models are used to investigate the absorption of SO_2 by calcined limestone. Particular emphasis is placed on the investigation of the combined effects of pore closure and formation of inaccessible volume on the evolution of the solid's reactivity and of its sorptive capacity for SO_2 removal.

Development of the Mathematical Models

A noncatalytic gas-solid reaction with formation of solid product has the general form

$$S(\text{solid}) + \nu_A A(\text{gas}) + \ldots \rightarrow \nu_P P(\text{solid}) + \ldots \quad \text{(R1)}$$

where ... denotes other gaseous species participating in the reaction. A typical example is the use of limestone and dolomite in the control of SO_2 emissions from fluidized-bed combustors. In the high-temperature environment of a combustor, the limestone particles undergo calcination, and the calcined product (mainly CaO) reacts with the gas according to the reaction

$$\text{CaO(solid)} + \text{SO}_2 + 1/2\text{O}_2 \rightarrow \text{CaSO}_4\text{(solid)} \quad \text{(R2)}$$

forming calcium sulfate. The mathematical modeling and analysis of gas-solid reactions with solid product is mostly complicated by the formation of the solid product and its deposition on the unreacted solid. Depending on the relative rates of reaction and diffusion in the porous structure, significant concentration gradients may exist in the intraparticle region, in which case both a structural model and a diffusion and reaction model are needed to describe the behavior of the reacting particles.

Structural models

We consider a three-dimensional lattice consisting of sites and bonds with coordination number, z, which is defined as the average number of bonds emanating from a site. We construct the initial ($t = 0$) pore structure of the solid by considering that the bonds of the lattice serve as axes of cylindrical pores of distributed size in the range $[R_{o*}, R_o^*]$. We describe the population of bonds, and consequently of the corresponding cylinders, using the distribution density $\ell_o(R_o)$, where $\ell_o(R_o)dR_o$ denotes the length of bonds per unit volume that are axes to pores in the size range $[R_o, R_o + dR_o]$. Notice that no assumption about the length of the bonds (axes) and its distribution has yet been made. At conversion levels different than zero, the internal structure of the reacting solid is characterized by two receding surfaces, the reaction surface (reacted-unreacted solid interface) and the gas-solid interface (pore surface). Each point of the reaction surface moves in the direction normal to it, with velocity proportional to the local reaction rate. Sotirchos and Yu (1985) built their model on the assumption that points of the reaction surface of the same curvature move with the same velocity, while an analogous assumption was made for the pore surface. A direct consequence of these two assumptions is that the reaction and pore surfaces of the solid structure can be represented by two populations of overlapping cylinders that are coaxial to those forming the initial pore structure. At the outset of the reaction all pores (bonds) are open, and no inaccessible pores exist. As the conversion increases, the average pore size diminishes if the stoichiometric volume ratio, Z, is greater than one. It is assumed that a pore becomes plugged (closed) if its radius reaches a critical threshold, R_{pc}. The smallest pores (with initial size R_{o*}) close first, at time t_*, and other pores follow. After pore closure takes place, open, inaccessible pores start to appear in the pore network. (An open, inaccessible pore is a pore segment of radius greater than R_{pc} which either has both ends closed, that is, it terminates at sites of closed pores, or belongs to a finite cluster of open pores.) Open, inaccessible pores are closed to diffusion, and hence the part of the reaction surface that is primarily accessed through them does not contribute significantly to the total reaction rate.

Let $R_p(R_o, t)$ denote the radius of an open, accessible pore at time t that has evolved from an initial pore of radius R_o. The radius of the corresponding capillary for the reaction surface is denoted by $R_r(R_o, t)$. At reaction times less than t_*, only open, accessible pores exist in the porous network, with distribution density $\ell_p^a(R_p, t)$ in the range $[R_{p*}, R_p^*]$. For $t > t_*$, on the other hand, the pore space of the solid is characterized by three kinds of pores (also see Yortsos and Sharma, 1984): open, accessible pores with density function $\ell_p^a(R_p, t)$ in $[R_{pc}, R_p^*]$, open, inaccessible pores with density function $\ell_p^n(R, t)$ in $[R_{pc}, R_p(R_o^*, t_*)]$, and closed (plugged) pores with length density function $\ell_p^b(R, t) = L_{po}^b(t)\delta(R - R_{pc})$, i.e., pores of radius R_{pc} with length per unit volume L_{po}^b. The population of capillaries used to represent the reaction surface is also divided into open, accessible capillaries; open, inaccessible capillaries; and capillaries that are coaxial to plugged pores.

We now define the distribution density $\ell_o^a(R_o, t)$, where $\ell_o^a(R_o, t)dR_o$ is the length of axes of pores of initial size in the range $[R_o, R_o + dR_o]$ that are open and accessible at time t. (For infinitely long cylindrical capillaries [Sotirchos and Yu, 1985], $\ell_o^a(R_o, t) \equiv \ell_o(R_o)$ since formation of inaccessible pores

does not take place.) From the definitions of $\mathfrak{L}_p^a(R_p, t)$ and $\mathfrak{L}_o^a(R_o, t)$ it follows that

$$\int_{R_p} \mathfrak{L}_p^a(R_p, t)dR_p = \int_{R_o} \mathfrak{L}_o^a(R_o, t)dR_o$$

for all $R_p(R_o, t)$. Differentiating the above expression with respect to R_o, we obtain

$$\mathfrak{L}_p^a(R_p, t) = \mathfrak{L}_o^a(R_o, t)/(\partial R_p/\partial R_o) \tag{1}$$

A similar expression is obtained for the corresponding distribution density $\mathfrak{L}_r^a(R_r, t)$ that describes the open, accessible capillaries of the reaction surface. In the following paragraphs equations that describe the evolution of $\mathfrak{L}_p^a(R_p, t)$, $\mathfrak{L}_p^n(R, t)$, and $L_{po}^b(t)$ are developed. Similar equations hold for the evolution of the corresponding functions for the reaction surface, which can readily be obtained by simply replacing subscript p by r.

Equations for $\mathfrak{L}_p^a(R_p, t)$, $\mathfrak{L}_p^n(R, t)$, and $L_{po}^b(t)$

Percolation theory is used to compute the number fraction of open, accessible pores, X^a, as a function of the total fraction of open pores, X. Broadbent and Hammersley (1957) introduced percolation theory as a branch of mathematical physics that describes the interaction of classical particles with a random medium. Percolation theory has found extensive use in the abstract description of the morphology and conductivity of disordered media. The functional relationship between X^a and X, $X^a(X)$ serves as a measure of the accessibility of the network (Shante and Kirkpatrick, 1971; Larson et al., 1981; Yortsos and Sharma, 1984) and is known for a given lattice. Each pore in the network is characterized by its radius and the length of the bond around which it is built. To facilitate the development of the model equations, we assume that the length of pore axes is distributed independently of the pore size. The number fraction of pores in some size range is then equal to their length fraction. The number fraction of open pores, $X(t)$, is equal to $(1 - L_{po}^b/L_o)$ where L_i is the ith moment of the initial density function, $\mathfrak{L}_o(R_o)$, and L_i is the ith moment of the density function $\mathfrak{L}$. Obviously,

$$L_{po}^b + L_{po}^n + L_{po}^a = L_o \tag{2}$$

Discrete Distribution of Pore Size. We first examine a discrete pore system with initial pore radii $R_{oi}(i = 1, \ldots N)$ and with density function

$$\mathfrak{L}_o(R_o) = \sum_{i=1}^{N} \mathfrak{L}_{oi}\delta(R_o - R_{oi}) \tag{3}$$

Let $[\mathfrak{L}_p^a(R_p)]_M$ be the length density function of open, accessible pores after the pores of initial size R_{oM} close and let $[\mathfrak{L}_p^n(R)]_M$ be the corresponding length density of inaccessible, open pores. We have then that

$$[\mathfrak{L}_p^a(R_p)]_M = \sum_{i=M+1}^{N} (\mathfrak{L}_{pi}^a)_M\delta(R_p - R_{pi}) \tag{4}$$

and

$$[\mathfrak{L}_p^n(R)]_M = \sum_{i=1}^{M}\sum_{j=i+1}^{N} (\mathfrak{L}_{pj}^n)_i\delta[R - (R_{pj})_i] \tag{5}$$

In Eq. 4 $(\mathfrak{L}_{pi}^a)_j$ stands for the length per unit of volume of open, accessible pores of initial size R_{oi} after the R_{oj} pores close, while in Eq. 5 $(\mathfrak{L}_{pi}^n)_j$ denotes the length per unit of volume of inaccessible pores of radius $(R_{pi})_j$ formed from the ith pore size when the pores of initial size R_{oj} close.

According to the above definitions, the total number fraction of open pores in the network following closure of pores of initial size R_{oM} is

$$X_M = 1 - \sum_{i=1}^{M} (\mathfrak{L}_{pi}^a)_{i-1} \Big/ \sum_{i=1}^{N} \mathfrak{L}_{oi} \tag{6}$$

On the other hand, if pore closure were occurring randomly over both accessible and inaccessible pores, the number fraction of open pores would be given by:

$$\hat{X}_M = 1 - \sum_{i=1}^{M} \mathfrak{L}_{oi} \Big/ \sum_{i=1}^{N} \mathfrak{L}_{oi} \tag{6a}$$

The total length fraction, or equivalently the number fraction, of open, inaccessible pores is equal to

$$(L_{po}^n)/L_o = X_M - X^a(\hat{X}_M) \tag{7}$$

where X^a is the accessibility function of the network. When the next pore size closes, an additional fraction that is equal to $[(L_{po}^n)_{M+1} - (L_{po}^n)_M/L_o]$ becomes inaccessible. This process occurs at random and involves the still active pore sizes R_{oM+2}, $\ldots R_{oN}$. Therefore,

$$(\mathfrak{L}_{pi}^a)_{M+1} = (\mathfrak{L}_{pi}^a)_M \left\{1 - \frac{[(L_{po}^n)_{M+1} - (L_{po}^n)_M]}{\sum_{j=M+2}^{N} (\mathfrak{L}_{pj}^a)_M}\right\};$$
$$i = M + 2, \ldots N \tag{8}$$

The length of open, inaccesible pores of radius $(R_{pi})_{M+1}$ formed at the above time instant is equal to

$$(\mathfrak{L}_{pi}^n)_{M+1} = (\mathfrak{L}_{pi}^a)_M - (\mathfrak{L}_{pi}^a)_{M+1}; \quad i = M + 2, \ldots N \tag{9}$$

Before pore closure starts, we obviously have that $(\mathfrak{L}_{pi}^a)_0 = \mathfrak{L}_{oi}$ and $(L_{po}^n)_0 = 0$.

Equations 2 and 4–9 give all the information needed for the computation of functions $\mathfrak{L}_p^a(R_p, t)$, $\mathfrak{L}_p^n(R, t)$, and $L_{po}^b(t)$ provided that function $R_p(R_o, t)$ is known.

Continuous Distribution of Pore Size. Similar equations, in differential form, are derived for a continuous pore size distribution. Let $R_c(t)$ denote the lower limit of the active initial pore size range at time t. At $R_o = R_c(t)$, we obviously have that $R_p(R_c(t), t) = R_{pc}$. Differentiating the last equation, we obtain

the differential equation

$$\frac{dR_c}{dt} = \begin{cases} 0 \text{ if } R_p(R_c, t) > R_{pc} \\ -\left(\frac{\partial R_p}{\partial t}\middle/\frac{\partial R_p}{\partial R_o}\right)\Big|_{R_o=R_c(t)} \text{ if } R_p(R_c, t) = R_{pc} \end{cases} \quad (10)$$

with $R_c(0) = R_{o*}$.

Consider the pore size range $[R_p, R_p^*]$. Inaccessible pores formed at time t in this size range obviously result from accessible pores in the same size range. This observation leads to the population balance

$$\left\{\frac{\partial}{\partial t}\left[\int_{R_p}^{R_p^*} \mathfrak{L}_p^a(R'_p, t)\, dR'_p\right]\right\}_{R_o} = -\frac{d}{dt}\left[\int_{R_p}^{R_p^*} \mathfrak{L}_p^n(R, t)\, dR\right] \quad (11)$$

Differentiating under the integral, we obtain the differential equation

$$\frac{\partial}{\partial t}\mathfrak{L}_p^a(R_p, t) + \frac{\partial}{\partial R_p}\left[\mathfrak{L}_p^a(R_p, t)\left(\frac{\partial R_p}{\partial t}\right)_{R_o}\right] = -\frac{\partial}{\partial t}\mathfrak{L}_p^n(R_p, t) \quad (12)$$

The population balance for the pore size range $[R_{pc}, R_p]$ is of the form

$$\left\{\frac{\partial}{\partial t}\left[\int_{R_{pc}}^{R_p} \mathfrak{L}_p^a(R'_p, t)\, dR'_p\right]\right\}_{R_o} = -\frac{d}{dt}\left[\int_{R_{pc}}^{R_p} \mathfrak{L}_p^n(R, t)\, dR\right] - \frac{dL_{po}^b}{dt} \quad (13)$$

Carrying out the differentiations in Eq. 13 and using Eq. 12, one obtains the equation

$$\frac{dL_{po}^b}{dt} = -\left(\frac{\partial R_p}{\partial t}\right)\mathfrak{L}_p^a(R_p, t)\Big|_{R_o=R_c(t)} \quad (14)$$

Since inaccessible pores in $[R_p, R_p^*]$ are formed at random (at time t) from open, accessible pores belonging to the same pore size range, we must have that

$$-\frac{d}{dt}\left[\int_{R_p}^{R_p^*} \mathfrak{L}_p^n(R, t)\, dR\right] \propto \int_{R_p}^{R_p^*} \mathfrak{L}_p^a(R'_p, t)\, dR'_p \quad (15)$$

The proportionality constant in Eq. 15 is a function of time only. An expression for it can be obtained by applying Eq. 15 to the size range $[R_{pc}, R_p^*]$. Differentiating under the integrals, rearranging, and using the expression for the proportionality constant, Eq. 15 becomes

$$\frac{\partial}{\partial t}[\mathfrak{L}_p^n(R_p, t)] = \left[\left(\frac{dL_{po}^n}{dt}\right)\left(\frac{1}{L_{po}^a}\right)\right]\mathfrak{L}_p^a(R_p, t) \quad (16)$$

Equations 12, 14, and 16 are similar to those derived by Yortsos and Sharma (1984). Most differences come from the fact that in our structural model the growth rate of the pores is a function of their initial size also.

Equation 16 may be used to eliminate $\mathfrak{L}_p^n$ from Eq. 12. Transforming the independent variables of the resulting differential equations from (R_p, t) to (R_o, t), we obtain the differential equation

$$\frac{\partial}{\partial t}\left[\mathfrak{L}_p^a(R_p, t)\left(\frac{\partial R_p}{\partial R_o}\right)\right]_{R_o} = \left[-\left(\frac{dL_{po}^n}{dt}\right)\left(\frac{1}{L_{po}^a}\right)\right]\mathfrak{L}_p^a(R_p, t)\left(\frac{\partial R_p}{\partial R_o}\right) \quad (17)$$

Equation 17 may readily be integrated to get

$$\mathfrak{L}_p^a(R_p, t) = \left[\frac{\mathfrak{L}_o(R_o)}{\partial R_p/\partial R_o}\right]\exp\left[-\int_o^t\left(\frac{dL_{po}^n}{dt}\right)\frac{1}{L_{po}^a}\,dt\right] \quad (18)$$

Integrating Eq. 18 over the active pore range $[R_c, R_o^*]$, or equivalently $[(R_{pc} \text{ or } R_{p*}), R_p^*]$, we get the equation

$$L_{po}^a = L_o(>R_c)\exp\left[-\int_o^t\left(\frac{dL_{po}^n}{dt}\right)\frac{1}{L_{po}^a}\,dt\right] \quad (19)$$

where $L_o(>R_c)$ is the total length per unit volume (zeroth moment) of pores of initial size greater than R_c.

If only the moments of $\mathfrak{L}_p^n(R, t)$ are needed, multiplication of both sides of Eq. 16 by R_p^k and subsequent integration give the equation

$$\frac{d}{dt}L_{pk}^n = \left(\frac{dL_{po}^n}{dt}\frac{1}{L_{po}^a}\right)L_{pk}^a; \quad k = 0, 1, \ldots \quad (20)$$

For $k = 0$, Eq. 20 is obviously an identity. To complete Eqs. 18 and 20, we need equations for $L_{po}^a(t)$ and $L_{po}^n(t)$. Equation 14 or 19 is used as one of these equations. (Notice that Eq. 19 is equivalent to Eq. 14 since differentiating Eq. 19, using Eq. 2, and rearranging one obtains Eq. 14.) The other equation is provided by the accessibility of the network. For a continuous distribution of pore size, Eq. 7 takes the form

$$L_{po}^n/L_o = X(t) - X^a[\hat{X}(t)] \quad (21)$$

where $X(t) = [L_{po}^n + L_{po}^a]/L_o$ and $\hat{X}(t) = L_o(>R_c)/L_o$.

Equations 18, 20, 21, and 14 or 19 provide a complete description of the evolution of $\mathfrak{L}_p^a(R_p, t)$, $\mathfrak{L}_p^n(R, t)$, and $L_{po}^b(t)$ for known $R_p(R_o, t)$. At $t = 0$, we obviously have that $\mathfrak{L}_p^a(R_p, t) = \mathfrak{L}_o(R_o)$ and $\mathfrak{L}_p^n(R, t) = 0$.

Equations for $R_r(R_o, t)$ and $R_p(R_o, t)$

To derive differential equations describing the evolution of functions $R_p(R_o, t)$ and $R_r(R_o, t)$, we follow a procedure similar to that used by Sotirchos and Yu (1985). For a first-order reaction, the reaction rate at points of curvature R_r is written

$$\frac{\partial R_r}{\partial t} = v_S k_s c_r \quad (22)$$

where c_r is the concentration at the reaction surface (reacted-unreacted solid interface). In order to preserve the cylindrical shape of the capillaries of the pore and reaction surface, we assume that c_r is uniform at points of the same curvature. The value of c_r is found by solving the diffusion equation in the product layer under pseudosteady-state conditions.

We define the distribution density $\sigma_{r,p}^a(R_o, t)$ where $\sigma_{r,p}^a(R_o, t)dR_o$ is the accessible reaction or pore surface area per unit volume that belongs to pores originating from the initial pore size range $[R_o, R_o + dR_o]$. Let us consider the product layer surrounding accessible pores originating from the above pore size range. The diffusion surface at position R $(R_p < R < R_r)$ must be equal to $\sigma_{r,p}^a(R_o, t')\{[\mathfrak{L}_o^a(R_o, t)]/[\mathfrak{L}_o^a(R_o, t')]\}dR_o$ where t' is the time instant at which $R_{r,p}(R_o, t') = R$. Using this observation and our assumption of uniform concentration at points of the same curvature, solution of the diffusion equation in the product layer surrounding active pores that originate from the range $[R_o, R_o + dR_o]$ gives, after

introducing the result in Eq. 22,

$$\frac{\partial R_r}{\partial t} = \frac{v_S k_s c_p}{1 + \dfrac{\nu_A k_s}{D_P}\dfrac{\sigma_r^a(R_o, t)}{\ell_o^a(R_o, t)}\displaystyle\int_{R_p}^{R_r}\frac{\ell_o^a(R_o, t')}{\sigma_{r,p}^a(R_o, t')}\,dR} \tag{23}$$

The equation for $R_p(R_o, t)$ is derived from a differential mass balance on the solid product assuming that the solid product formed from reaction on the reaction surface that belongs to accessible capillaries in the initial size range $[R_o, R_o + dR_o]$ is deposited as a layer of uniform thickness on the surface of open, accessible pores that originate from the same initial size range. We have

$$\frac{\partial R_p}{\partial t} = -\frac{\partial R_r}{\partial t}\left[(Z-1)\frac{\sigma_r^a(R_o, t)}{\sigma_p^a(R_o, t)}\right] \tag{24}$$

The initial conditions associated with Eqs. 23 and 24 are $R_r(R_o, 0) = R_p(R_o, 0) = 0$.

An overall mass balance on the solid product and solid reactant gives

$$\epsilon_r = \epsilon_o + (\epsilon_o - \epsilon_p)/(Z-1) \tag{25}$$

where ϵ_p is the porosity of the solid and ϵ_r is the porosity of the reaction surface structure. Equation 25 can also be expressed in terms of the conversion of the solid as

$$\xi = \frac{\epsilon_o - \epsilon_p}{(Z-1)(1-\epsilon_o)} \tag{26}$$

To proceed further we need equations relating the distribution density functions $\sigma_{r,p}^a(R_o, t)$ and the porosities of the reaction and pore surface structures, ϵ_r and ϵ_p, to the length density functions $\ell_p^a(R_p, t)$, $\ell_p^n(R, t)$, etc. Let us consider the initial pore structure. The total volume of cylinders per unit volume is obviously given by the relation

$$\epsilon_{ox} = \pi\int_{R_{o^*}}^{R_o^*} R_o^2\ell_o(R_o)dR_o \tag{27}$$

The above quantity is larger than the porosity of the pore network since its computation does not allow for pore overlapping. Similarly, the total surface area of the cylinders per unit volume,

$$S_{ox} = 2\pi\int_{R_{o^*}}^{R_o^*} R_o\ell(R_o)dR_o \tag{28}$$

is larger than the internal surface area of the porous structure.

In order to derive equations relating ϵ_{ox} and S_{ox} to the porosity, ϵ_o, and surface area, S_o, it is assumed that the structural properties of the pore network constructed above can be approximated, and vice versa, by those of a population of finite cylindrical pores of the same length distribution density, $\ell_o(R_o)$, randomly distributed in the three-dimensional space. Avrami's (1940) analysis of phase transformation systems, used to describe the structural properties of a random pore or grain system (Bhatia and Perlmutter, 1980; Sotirchos, 1986), can now be used to obtain structural relationships for the pore network considered in this study. It is shown (Avrami, 1940; Sotirchos, 1986) that

$$\epsilon_o = 1 - \exp(-\epsilon_{ox}) \tag{29}$$

$$S_o = (1-\epsilon_o)S_{ox} \tag{30}$$

Introducing Eqs. 1 and 2 in Eqs. 3 and 4, we obtain the equations

$$\epsilon_o = 1 - \exp\left[-\pi\int_{R_{o^*}}^{R_o^*} R_o^2\ell_o(R_o)dR_o\right] \tag{31}$$

$$S_o = 2\pi(1-\epsilon_o)\int_{R_{o^*}}^{R_o^*} R_o\ell_o(R_o)dR_o \tag{32}$$

which turn out to be identical to those of the random-pore model developed by Gavalas (1980) and Bhatia and Perlmutter (1980). This is not surprising since the structural properties given by Eqs. 29 and 30 depend only on the total values of the extended pore volume, ϵ_{ox}, and surface area, S_{ox}, and not on how these quantities are distributed among the various geometrical objects used to represent the void space of the solid.

Equations 29 and 30 may be used to obtain the total porosity and surface area of the pore or reaction surface structure at time t. We have that

$$\epsilon_p = 1 - \exp\left[-\pi\int_{R_{pc}}^{R_p^*} R_p^2\ell_p^a(R_p, t)dR_p\right] \cdot \exp\left[-\pi\int_{R_{pc}}^{R_p(R_o^*, t^*)} R^2\ell_p^n(R, t)dR\right] \cdot \exp(-\pi R_{pc}^2 L_{po}^b) \tag{33}$$

and

$$S_p = 2\pi(1-\epsilon_p)\left[\int_{R_{pc}}^{R_p^*} R_p\ell_p^a(R_p, t)dR_p + \int_{R_{pc}}^{R_p(R_o^*, t^*)} R\ell_p^n(R, t)dR + R_{pc}L_{po}^b\right] \tag{34}$$

The internal surface area that belongs to open, accessible pores is given by the expression

$$S_p^a = 2\pi(1-\epsilon_p)\left[\int_{R_{pc}}^{R_p^*} R_p\ell_p^a(R_p, t)dR_p\right] \tag{35}$$

and the distribution density $\sigma_p^a(R_o, t)$, is given by

$$\sigma_p^a(R_o, t) = 2\pi(1-\epsilon_p)R_p\ell_o^a(R_o, t) \tag{36}$$

Notice that only the first two moments of the distribution density $\ell_p^n(R, t)$ are needed. Equations similar to Eqs. 33–36 also hold for the corresponding quantities and density functions used to describe the reaction surface.

We must again point out that the above equations provide only approximations to the structural properties of the pore network considered here, inasmuch as they rigorously apply only to randomly distributed pore segments in the three-dimensional space.

Equations 33 to 36 may readily be modified for application to a network of discrete distribution of pore size. For instance, the porosity of the network, ϵ_p, after pores of initial size R_{oM} close is given by the expression (compare to Eq. 33)

$$(\epsilon_p)_M = 1 - \exp\left[-\pi \sum_{i=M+1}^{N} R_{pi}^2 (\mathcal{Q}_{pi}^a)_M\right] \cdot \exp\left[-\pi R_{pc}^2 \sum_{i=1}^{M} (\mathcal{Q}_{pi}^a)_{i-1}\right] \cdot \exp\left[-\pi \sum_{j=1}^{M} \sum_{i=j+1}^{N} (R_{pi})_j^2 (\mathcal{Q}_{pi}^n)_j\right] \tag{37}$$

Introducing Eq. 36 in Eqs. 23 and 24, we get

$$\frac{\partial R_r}{\partial t} = \frac{v_S k_s c_p}{1 + \dfrac{\nu_A k_s}{D_p}(1 - \epsilon_r) R_r \displaystyle\int_{R_p}^{R_r} \frac{dR}{[1 - \epsilon_{r,p}(t')]R}} \tag{23a}$$

$$\frac{\partial R_p}{\partial t} = -\frac{\partial R_r}{\partial t}\left[(Z - 1)\frac{(1 - \epsilon_r)}{(1 - \epsilon_p)}\frac{R_r}{R_p}\right] \tag{24a}$$

For a discrete pore size distribution of N pore sizes, Eqs. 23a and 24a yield $2N$ ordinary differential equations, two for each pore size. In addition to eqs. 23a and 24a, the structural model for a discrete distribution of pore size also includes Eqs. 6–9 for $\mathcal{Q}_p^a$, $\mathcal{Q}_p^n$, and L_{po}^b and Eqs. 37 and 25 for ϵ_p and ϵ_r. The structural model for a continuous distribution, on the other hand, is described by two partial integrodifferential equations, Eqs. 23a and 24a, defined over the range $[R_c(t), R_o^*]$; Eqs. 18, 20 (for $k = 1, 2$), Eq. 21 and Eq. 14 or 19 for $\mathcal{Q}_p^a$, the moments of $\mathcal{Q}_p^n$, and L_{po}^b; Eq. 10 for $R_c(t)$; and Eqs. 33 and 25 for ϵ_p and ϵ_r.

Diffusion and reaction model

If significant intraparticle gradients of concentration exist, a diffusion and reaction model is needed along with either of the structural models (discrete or continuous) developed in the previous section. For spherical particles of radius a, the mass balance equation for the gaseous reactant A (Fick's law and no Stefan flow effects) is written

$$\epsilon_p^a(\xi)\frac{\partial c_p}{\partial t} = \frac{1}{r^2}\frac{\partial}{\partial r}\left[r^2 D^e(\xi)\frac{\partial c_p}{\partial r}\right] - \nu_A R_v(\xi, c_p) \tag{38}$$

The mass balance for the solid has the form

$$\frac{\partial \xi}{\partial t} = \frac{v_S}{(1 - \epsilon_o)} R_v(\xi, c_p) \tag{39}$$

The following boundary and initial conditions are used:

$$\text{at } r = 0: \quad \frac{\partial c_p}{\partial r} = 0 \tag{40a}$$

$$\text{at } r = a: \quad k_g(c_f - c_p) = D^e \frac{\partial c_p}{\partial r} \tag{40b}$$

$$\text{at } t = 0: \quad c_p = 0 \quad \text{and} \quad \xi = 0 \tag{40c}$$

The porosity ϵ_p^a, the diffusion coefficient D^e, and the reaction rate per unit volume, R_v, are functions of the local conversion. Their values are found by solving independently the structural model equations developed in the previous section. The effective diffusivity is estimated using the Feng-Stewart model (Feng and Stewart, 1973; Jackson, 1977), applied to the accessible pore size distribution. We have that

$$D^e(\xi) = (1/\eta)\int_{(R_p^* \text{or} R_{pc})}^{R_p^*} D_A(R_p)\epsilon_p^a(R_p, t')dR_p \tag{41}$$

where $\epsilon_p^a(R_p, t')$ is the porosity density function of accessible pores at time t' corresponding to local conversion ξ. For a discrete pore size distribution, we have, after closure of the Mth pores takes place (Gavalas, 1980; Sotirchos and Yu, 1985),

$$[\epsilon_p^a(R_p, t)]_M = \sum_{i=M+1}^{N} (\epsilon_{pi}^a)_M \delta(R_p - R_{pi}) \tag{42}$$

where

$$(\epsilon_{pi}^a)_M = \exp\left[-\pi \sum_{j=i+1}^{N} (\mathcal{Q}_{pj}^a)_M R_{pj}^2\right] - \exp\left[-\pi \sum_{j=1}^{N} (\mathcal{Q}_{pj}^2)_M R_{pj}^2\right]$$

For a continuous distribution of pore size, on the other hand, the porosity density function is given by

$$\epsilon_p^a(R_p, t) = \pi R_p^2 \mathcal{Q}_p^a(R_p, t) \exp\left[-\pi \int_{R_p}^{R_p^*} R^2 \mathcal{Q}_p^a(R, t)dR\right] \tag{43}$$

$D_A(R)$ is the diffusivity of A in a capillary of radius R given by

$$\frac{1}{D_A(R)} = \frac{1}{\mathcal{D}} + \frac{1}{D_K(R)} \tag{44}$$

The reaction rate per unit volume is computed by averaging the reaction rate at a point of curvature R_r, Eq. 23a, over all active pores, that is, by using the expression

$$R_v(\xi, c_p) = \left(\frac{1}{v_S}\right)\int_{R_c}^{R_o^*}\left(\frac{\partial R_r}{\partial t}\right)\sigma_r^a(R_o, t')dR_o \tag{45}$$

It must be pointed out that Eq. 41 is based on the so-called smooth field approximation (Jackson, 1977), which may violate the mass balance for species A at the nodes of the pore network (Sotirchos and Burganos, 1986). Nevertheless, we will employ Eq. 41 for the estimation of the intraparticle diffusivity so as to make our computational results comparable with those obtained in our previous study (Sotirchos and Yu, 1985).

Computational Aspects

The numerical procedure used for the structural model is similar to that used by Sotirchos and Yu (1985). For a continuous pore size distribution, the model equations are discretized using spline collocation (de Boor, 1978) over a spacelike variable, R_o. The resulting system of ordinary differential and algebraic equations is integrated in time using a Gear-type integrator. The same integrator is used to integrate the ordinary and algebraic equations describing the discrete structural model. More details

about the procedure may be found in the paper by Sotirchos and Yu (1985), and an extensive discussion of the method is given by Yu (1986).

The equations for the diffusion and reaction model Eqs. 38 and 39, are solved by combining spline collocation in space and the ensuing integration of the resulting ordinary differential equations in time (Sotirchos and Yu, 1985; Yu, 1986).

Results and Discussion

The results that we present in the following paragraphs are for calcined limestone particles, mainly composed of CaO, reacting in an environment containing SO_2 and O_2. The stoichiometric volume ratio of the system, as the data of Table 1 show, is much greater than one, and hence pore closure behavior is exhibited by the system. The critical pore size at which pore closure occurs is taken equal to 10 Å (1 nm), as in Sotirchos and Yu (1985), assuming that in pores of smaller size the dominant diffusion mechanism is slow activated diffusion. The rate of the chemical reaction is considered to be first order with respect to the concentration of sulfur dioxide. Table 1 reports average values of physical and kinetic data for the CaO—SO_2 system compiled by Sotirchos and Yu (1985) from a number of experimental studies (Borgwardt, 1970; Hartman and Coughlin, 1974, 1976; Ulerich et al., 1977). Both discrete and continuous distributions of pore size are employed in our numerical simulations. For discrete systems, the initial length density function

$$\ell_o(R_o) = \sum_{i=1}^{N} \ell_{oi}\delta(R_o - R_{oi})$$

is obtained from the porosity density function

$$\epsilon_o(R_o) = \sum_{i=1}^{N} \epsilon_{oi}\delta(R_o - R_{oi})$$

through the relation (Gavalas, 1980; Sotirchos and Yu, 1985)

$$\ell_{oi} = \frac{1}{\pi R_{oi}^2} \ln\left(\frac{1 - \sum_{j=i+1}^{N} \epsilon_{oj}}{1 - \sum_{j=i}^{N} \epsilon_{oj}}\right) \tag{46}$$

For a continuous distribution of pore size, on the other hand, $\ell_o(R_o)$ and $\epsilon_o(R_o)$ are related by the equation (compare to Eq. 43)

$$\ell_o(R_o) = \frac{\epsilon_o(R_o)}{\pi R_o^2\left[1 - \int_{R_o}^{R_o^*} \epsilon_o(R_o')dR_o'\right]} \tag{47}$$

Table 1. Physical, Kinetic, and Pore Structure Data Used

$v_S k_s = 4 \times 10^{-5}$ m^4/kmol · s
$v_S = 16.9 \times 10^{-3}$ m^3/kmol
$\epsilon_o = 0.5$
$D_P = 2 \times 10^{-12}$ m^2/s
$v_P = 52.2 \times 10^{-3}$ m^3/kmol
Reaction conditions: 1 atm; 850 °C; 0.3% SO_2, mol/mol

Before we proceed further, we must discuss the type of lattice chosen to serve as a skeleton of the porous medium and its accessibility. The porous medium we study is built around a Bethe lattice of coordination number z in the sense that the bonds of the lattice function as axes of the cylindrical pores of the network. Regular Bethe lattices are treelike structures with bonds emanating from sites of the same coordination number. Their main advantage over other types of lattices is that their topological properties can be determined analytically. Bethe tree lattices were also considered by Yortsos and Sharma (1984). The fraction of accessible bonds, and hence of pores for the corresponding pore system, is related to the total number of open bonds (open pores) by the equation (Fisher and Essam, 1961)

$$X^a(X) = \begin{cases} 0 \text{ if } X < X_c \\ X - X(X^*/X)^{(2z-2)/z-2)} \text{ if } X > X_c \end{cases} \tag{48a}$$

where

$$X^*(1 - X^*)^{z-2} - X(1 - X)^{z-2} = 0; \quad X^* < X \tag{48b}$$

The accessibility function of other lattices is usually found by computer simulation methods (Shante and Kirkpatrick, 1971; Stauffer, 1979). Equation 48 states that when the fraction of open pores, or equivalently the probability that a pore is open, drops below a nonzero threshold value, X_c, the so-called percolation threshold, no infinite cluster of pores that spans the porous medium is present, and hence intraparticle mass transport cannot take place. Above the percolation threshold, however, both finite (inaccessible) and infinite (accessible) clusters of pores exist. It follows from Eq. 48b that the percolation threshold for a Bethe tree is equal to $1/(z - 1)$ (Fisher and Essam, 1961). The variation of the accessibility fraction of a Bethe tree with the fraction of open bonds (accessible pores) is shown in Figure 1 for various coordination numbers.

We first discuss conversion vs. time results for particles reacting under conditions of insignificant intraparticle concentration gradients. In this case, the structural model completely describes the behavior of the reacting particles. The values of sulfur dioxide concentration and temperature used, shown in Table 1, are typical of limestone-SO_2 experiments. Figure 2 presents the effect of lattice coordination number on the conversion trajectories of particles with discrete bimodal distribution of pore size (500 and 1,000 Å; 50 and 100 nm). The dashed curve corresponds to the same solid reacting without formation of inaccessible volume according to the model developed by Sotirchos and Yu (1985). (The structural model equations that were developed in this study reduce to those of the above model for infinitely large coordination numbers.) The ultimate conversion reached by the particles reacting without formation of inaccessible volume is about 48%, as predicted by Eq. 16 for a gas-solid

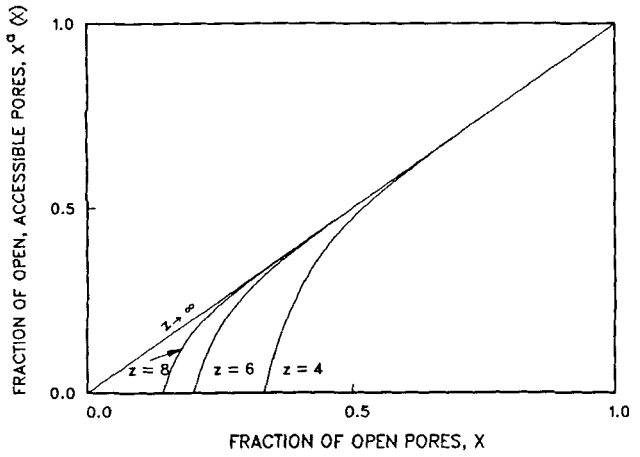

Figure 1. Accessibility of Bethe trees for various coordination numbers, Eq. 48.

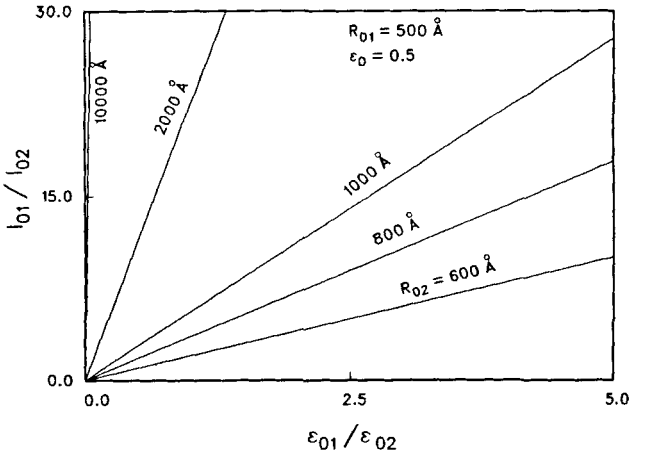

Figure 3. Length ratio ℓ_{o1}/ℓ_{o2} vs. porosity ratio $\epsilon_{o1}/\epsilon_{o2}$ for a bimodal pore system.

system with the properties of Table 1. As we decrease the value of the coordination number, the volume of inaccessible pore space formed when closure of the 500 Å pores occurs increases, and the maximum conversion attained by the solid decreases. For $z = 4$, no intraparticle mass transport, and hence no reaction, takes place in the interior of the reacting particles since the number fraction of open pores that is left after the small pores are blocked is below the percolation threshold of the system. Figure 3 presents the ratio of the lengths per unit volume of small and large pores as a function of the ratio of their porosities, Eq. 46. It is seen there that the corresponding ℓ_{o1}/ℓ_{o2} ratio for $\epsilon_{o1}/\epsilon_{o2} = 2/3$ is approximately 3.77. At the time the small pores close, therefore, the remaining number fraction of open bonds is $\ell_{o2}/(\ell_{o1} + \ell_{o2}) = 0.21$, which is well below the percolation threshold of a Bethe lattice for $z = 4$ but barely above that for $z = 6$.

The results shown in the following figures were obtained for coordination number equal to 6, unless it is mentioned otherwise. It should be kept in mind, however, that the coordination number of the skeleton of the porous network is among the most important parameters of the process. For a given distribution of pore size, the only parameter that determines the extent of formation of inaccessible volume is the network's coordination number. The effect of the porosity distribution between small and large pores ($\epsilon_{o1}/\epsilon_{o2}$) on the reaction trajectories followed by a limestone exhibiting bimodal distribution of pore size (500 and 1,000 Å) is studied in Figure 4. The number fraction of large pores, $\ell_{o2}/(\ell_{o1} + \ell_{o2})$, for this bimodal system becomes smaller than the percolation threshold of a Bethe lattice with $z = 6$ for $\epsilon_{o1} > 0.208$, Figure 3, and hence no reaction takes place after the small pores close, Figure 4. The dashed curves of Figure 4 present reaction trajectories for particles without inaccessible volume, which for obvious reasons eventually reach the maximum conversion that is stoichiometrically allowable for the system.

Some results that are very interesting, especially for applications, are shown in Figure 5, where the size of large pores and the distribution of porosity are allowed to change while the total porosity and surface area of the solid are kept constant. Usually, as is the case with most experimental results available in the literature, only the initial porosity and surface area of the reacting system are known (reported). Figure 5 clearly shows that such data are incomplete for reactor design and model testing since the behavior of the reacting particles is strongly influenced by the actual form of the pore size distribution. Decreasing the por-

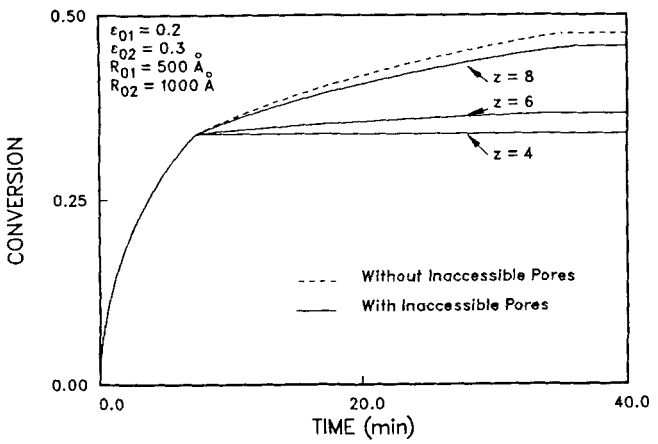

Figure 2. Dependence of conversion trajectories for a solid with discrete, bimodal distribution of pore size on the lattice coordination number.

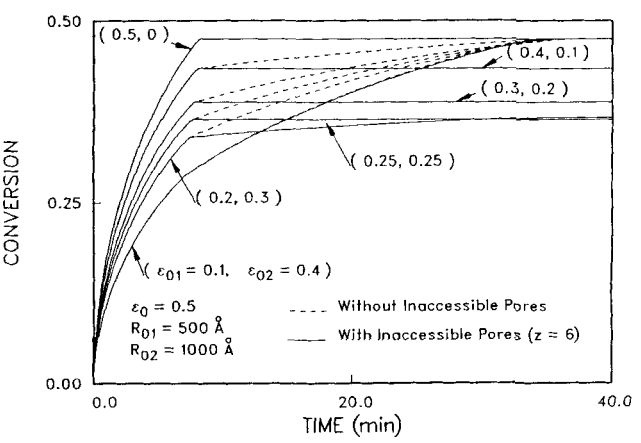

Figure 4. Conversion trajectories of a solid with discrete, bimodal distribution of pore size for several porosity ratios.

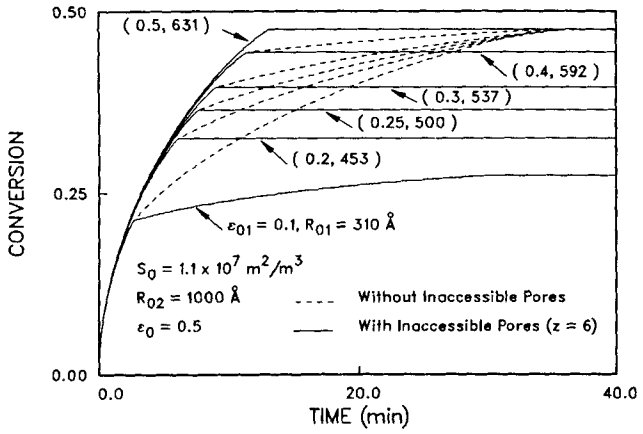

Figure 5. Effects of porosity distribution on conversion vs. time results for a solid of fixed initial porosity and internal surface area.

osity of large pores leads to higher maximum conversions as a result of the decreasing volume of inaccessible pore space formed when the small pores close. Notice again that for ϵ_{o1} values greater than 0.2 no intraparticle mass transport and reaction takes place after the 500 Å pores close. Comparing the reaction trajectories shown in Figures 2, 4, and 5 with the corresponding conversion vs. time (dashed) curves without formation of inaccessible volume (Sotirchos and Yu, 1985), we conclude that the form of the pore size distribution plays a considerably more important role in the overall reaction and pore structure evolution process if formation of inaccessible volume takes place. In the latter case, the pore size distribution determines not only the evolution of the rate of the reaction but also the value of maximum conversion that can be attained by the system, that is, the ultimate sorptive capacity of the limestone sample.

We now proceed with the presentation of reaction trajectories predicted by our structural model for solids with continuous distribution of pore size. Two types of continuous pore size distribution are considered: a Gaussian distribution with most probable size of 500 Å and standard deviation 100 Å, and a uniform distribution extending over the range [200, 1,000 Å]. Figure 6 presents the porosity, $\epsilon_o(R_o)$, and length, $\ell_o(R_o)$, density functions associated with the above distributions. The length density functions are computed from the porosity density functions using Eq. 47. Conversion vs. time results for the solid with Gaussian distribution of pore size are shown in Figure 7. If inaccessible volume is formed (solid curve), the solid reaches—as in the case of discrete distributions of pore size—maximum conversions lower than what is stoichiometrically allowable. The predicted differences between solids with and without inaccessible volume are not as large as those exhibited by limestones with bimodal pore size distribution, Figures 4 and 5. This is due to the fact that the porosity and the length density functions of the Gaussian distribution solid are not far different, Figure 6, and hence inaccessible volume is formed—as the pores start to close—at a relatively low rate. The length density function of the uniform pore size distribution, however, is markedly shifted toward the lower end of the pore size range. For this reason, as the small pores start to close the fraction of open pores decreases rapidly, and this leads to formation of relatively large inaccessible pore volume, Figure 8. Thus, notice that for $z = 6$ the ultimate conversion reached by the solid is about 0.37, compared to 0.48 if inaccessible pore space is not formed (dashed curve).

Figure 9 compares the porosity density functions of accessible pores with and without inaccessible volume for the solid with Gaussian distribution of pore size, Figure 6. At $t = 550$ s the solid with inaccessible pores practically exhibits no accessible pore volume in the interior. The behavior of the porosity density function of accessible pores, $\epsilon_p^a(R_p, t)$, for uniform distribution of initial pore size, Figure 10, is qualitatively similar to that for Gaussian distribution. Because of the formation of inaccessible pore volume, the accessible porosity density function of the percolating network is smaller than that of the pore network without inaccessible pore space (Sotirchos and Yu, 1985). The difference of the two density functions increases as the percolation threshold is approached. Before pore closure starts, the two networks are characterized by the same porosity density function.

The effects of intraparticle diffusional limitations on the behavior of the reacting solid particles are shown in Figures 11 and 12. Curves A correspond to the case without significant

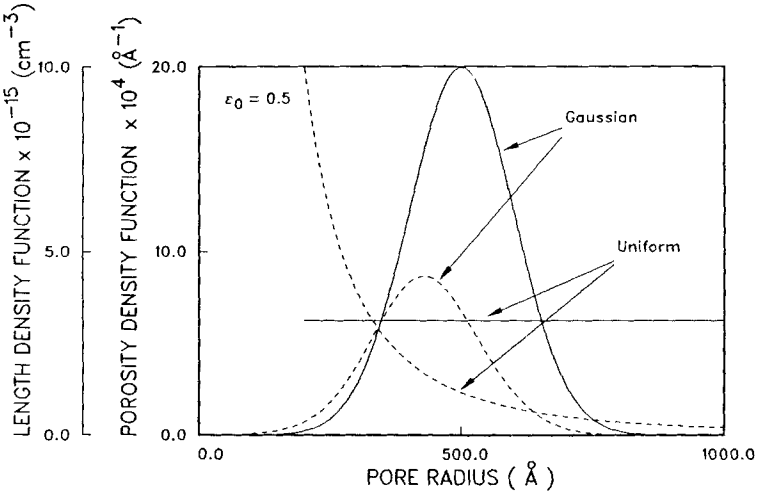

Figure 6. Density functions for Gaussian and uniform pore size distributions.
— porosity - - - - length

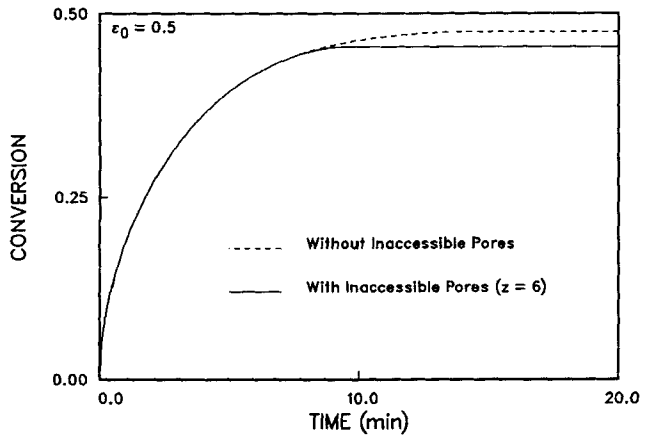

Figure 7. Effects of formation of inaccessible pores on reaction trajectories of a solid with Gaussian pore size distribution, Figure 6.

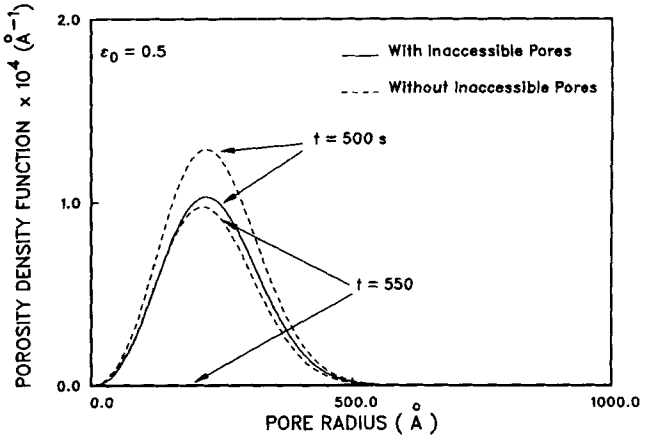

Figure 9. Evolution of porosity density of accessible pores for the solid of Figure 7.

intraparticle diffusional limitations, that is, for very small particles. Significant concentration gradients lead to higher reaction rates in the vicinity of the external surface of the porous particle during the initial stages of the reaction. Therefore, pore closure may first occur at the external surface preventing further mass transport and reaction in the interior. This in turn leads to a considerable decrease of the maximum conversion that can be reached by the reacting particles, and hence it significantly lowers their sorptive capacity. When closure of the small pores occurs at the external surface of the particles of Figure 11, the remaining fraction of open pores is below the percolation threshold, and consequently the gaseous reactant cannot enter the interior of the particles. However, the particles that do not form inaccessible volume (dashed curves) continue reacting until the pores of initial size of 1,000 Å close in the vicinity of the particle's external surface; as a result, they exhibit higher sorptive capacity. Increasing the particle size, the profiles of gaseous reactant concentration and solid conversion become steeper, leading to lower average conversions when pore plugging at the external surface takes place. The particle size effect on the conversion trajectories of particles with continuous distribution of pore size, Figure 12, is similar. Notice that for the conversion trajectories shown in Figures 11 and 12, pore plugging occurs at the same time instant in each figure. This is due to the fact that we are using infinitely large Sherwood numbers, and consequently the reaction conditions at the external surface do not depend on the intraparticle diffusion and reaction details.

The results presented in the preceding paragraphs point to the conclusion that the behavior of solid particles undergoing a reaction with solid product depends strongly on the type of the pore size distribution. Solids characterized by the same values of initial porosity and surface area may exhibit not only different reactivity evolution with time but also different maximum conversion because of the formation of inaccessible pore space. Because of the strong dependence of the results on the pore size distribution, it is practically impossible, even meaningless, to compare quantitatively the predictions of our mathematical models with experimental data for solids of poorly known distribution of pore size (see also Sotirchos and Yu, 1985), as is the case with most experimental studies presented in the literature. The predictions of our mathematical models qualitatively agree with experimental data presented in the literature (Hartman

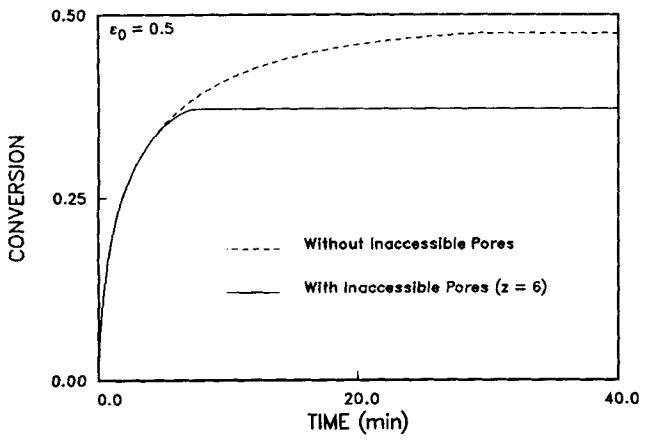

Figure 8. Effects of formation of inaccessible pores on conversion vs. time results for a solid with uniform distribution of pore size, Figure 6.

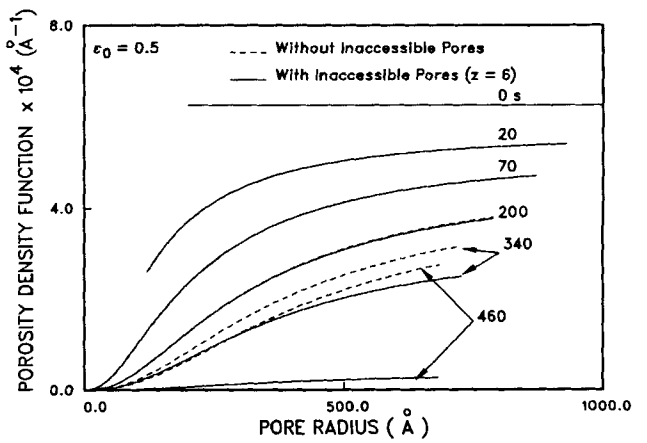

Figure 10. Evolution of porosity density of accessible pores for the solid of Figure 8.

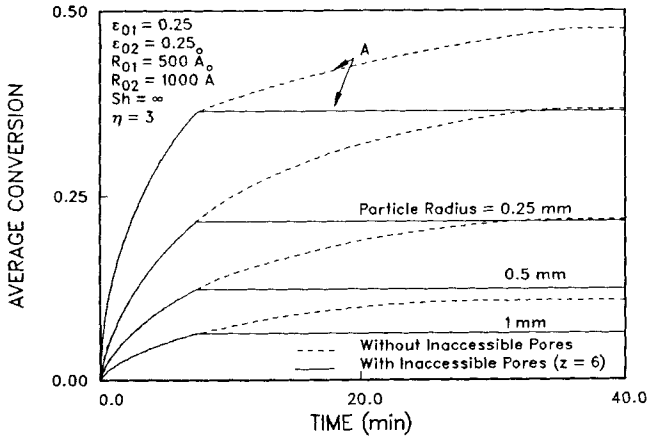

Figure 11. Effects of intraparticle diffusional limitations on average conversion vs. time results for a bimodal solid.

A, conversion trajectories without intraparticle concentration gradients.

and Coughlin, 1976), which also exhibit incomplete conversion and dependence of maximum conversion on particle size. The maximum conversion that is reached by the reacting solid in the kinetically controlled regime depends only on the coordination number of the pore network for a given pore size distribution. Therefore, the coordination number of the network can be estimated independently of the other parameters of the model by simply comparing the maximum conversion attained by the solid in the kinetically controlled regime with the stoichiometrically allowable maximum conversion, which is equal to $\epsilon_o/[(Z-1)(1-\epsilon_o)]$, Eq. 16.

Summary and Conclusions

General structural models are developed for the study of gas-solid noncatalytic systems with solid product under reaction conditions controlled by intrinsic kinetics and diffusion through the product layer. The reaction and pore surfaces of the reacting solid are represented by coaxial cylindrical capillary systems

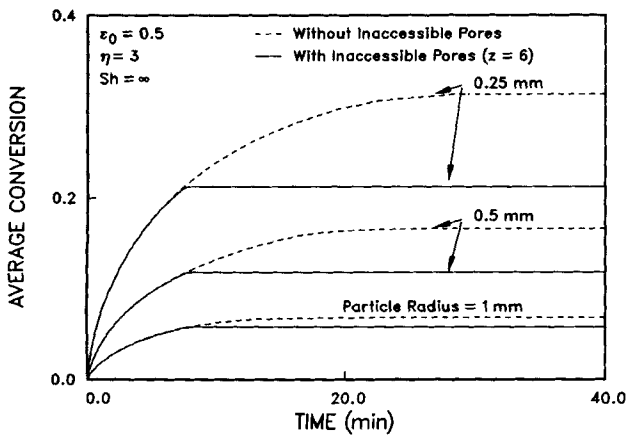

Figure 12. Particle size effects on reaction trajectories of the solid with uniform distribution of pore size, Figure 6.

built around a three-dimensional lattice, with the bonds of the lattice serving as axes of the capillaries. The coordination number of the lattice is treated as a model parameter, and percolation theory is used to determine the fraction of inaccessible pores formed after pore closure starts to take place. Specific model equations for the above capillary systems are derived by assuming that their structural properties (porosity, internal surface area, etc.) can be approximated by those obtained if the cylinders forming the pore network were randomly distributed in the three-dimensional space. Both discrete and continuous distributions of pore size are considered. When the gas-solid reaction occurs under significant intraparticle concentration gradients, a diffusion and reaction model is used along with the structural model for the description of the transient behavior of the system. The model equations, both for the structural and the diffusion and reaction models, are solved by discretization over a space-like variable, by spline collocation, followed by integration in time.

The developed mathematical models are used to investigate the transient behavior of calcined limestone particles reacting in an environment of sulfur dioxide. The calcined limestone SO_2 system is characterized by a stoichiometric volume ratio of product ($CaSO_4$) to reactant (CaO) greater than one, and hence it exhibits pore closure behavior. Our extensive computations showed that the formation of inaccessible volume depends on the coordination number of the pore network and on the form of the pore size distribution. For a solid of known pore size distribution, the coordination number may be estimated from the difference between the experimentally measured maximum conversion and the maximum conversion that is stoichiometrically allowable. The effects of the pore size distribution on the transient behavior of the reacting particles are very strong. Limestones characterized by the same initial values of porosity and internal surface area may exhibit not only dissimilar histories of reactivity evolution with the conversion, but also different ultimate conversions, that is, different sorptive capacities for SO_2 removal. In general, our simulation results revealed that the broader the pore size distribution of the solid, the larger the inaccessible pore volume formed in the interior.

Under conditions of significant concentration gradients in the interior of the reacting particles, the maximum conversion attained may decrease further. Depending on the relative rates of intraparticle diffusion and reaction, complete pore closure may first occur at the external surface of the solid particles while there is still open space in the interior. The maximum conversion attained by a certain noncatalytic gas-solid system that exhibits pore closure behavior depends, in general, on the form of the pore size distribution, the extent of the intraparticle diffusional limitations, the intrinsic reactivity of the solid, the particle size, and the ambient conditions. Most experimental studies that have appeared in the literature, however, do not present data on the evolution of the pore size distribution and of the effective diffusivity with the conversion. It is therefore relatively easy to reproduce satisfactorily the reactivity or conversion vs. time data reported in those studies by simply making suitable choices of the unknown parameters of the problem. We believe that more experimental information on the pore structure evolution and intraparticle mass transport processes is needed for testing mathematical models of gas-solid reactions in which pore closure and incomplete conversion phenomena arise.

Acknowledgment

This work has been supported in part by grants from the National Science Foundation and the Department of Energy.

Notation

a = radius of particle
c = concentration of reactant A
c_f = concentration of gas in bulk
D_P = diffusion coefficient in product layer
D^e = effective diffusion coefficient
$\mathcal{D}$ = bulk diffusion coefficient of species A
$D_K(R)$ = Knudsen diffusivity of A in a capillary of radius R
k_g = mass transfer coefficient
k_s = reaction rate constant
ℓ_i = length of axes per unit volume of ith group of capillaries in a discrete distribution
$\ell(R)dR, \ell(R, t)dR$ = length of axes of capillaries per unit volume in size range $[R, R + dR]$
$\ell_o^a(R_o, t)dR_o$ = length of axes of pores per unit volume of initial size in range $[R_o, R_o + dR_o]$ that are still accessible at time t
L_i = ith moment of $\ell_o(R_o)$
$L_o(>R_c)$ = zeroth moment of $\ell_o(R_o)$ in range $[R_c, R_o^*]$
L'_i = ith moment of density ℓ'
r = radial distance in particle
R = capillary radius
$R_c(t)$ = lower limit of active part of initial pore size range
R_i = ith capillary size in a discrete distribution ($i = 1, \ldots N$)
R_{pc} = critical pore size for pore closure
R_v = average local reaction rate per unit volume
$R(R_o, t)$ = radius of a capillary of initial size R_o at time t
S = internal surface area of capillary structure
t = time
t_* = time at which smallest pores close
v_i = specific molar volume of solid i
X = total number fraction of open pores
z = coordination number of lattice
Z = stoichiometric volume ratio ($\nu_P v_P / v_s$)

Greek letters

δ = Dirac delta function
ϵ = porosity of capillary structure
$\epsilon(R)dR, \epsilon(R, t)dR$ = pore volume in range $[R, R + dR]$
η = tortuosity factor
ν_i = stoichiometric coefficient of ith species
ξ = solid conversion
$\sigma(R)dR, \sigma(R, t)dR$ = surface area per unit volume in range $[R, R + dR]$

Subscripts

$1, \ldots N$ = ith capillary size of a discrete distribution
o = refers to $t = 0$
r = values at reaction surface or properties of reaction surface structure
p = values at pore surface or properties of pore structure
r, p = r or p, in this order
A = gaseous reactant
P = solid product
S = solid reactant
x = quantities computed without allowing for capillary overlapping
$*$ = lower limit of capillary size range
$(\cdot)_j$ = value of variable $\cdot$ after jth group of pores in a discrete distribution closes ($j = 0, 1, \ldots N$)

Superscripts

a = open, accessible pores
b = closed (plugged) pores
n = open, inaccessible pores
$*$ = upper limit of capillary size range

Literature cited

Avrami, M., "Kinetics of Phase Change. II: Transformation-Time Relations for Random Distribution of Nuclei," *J. Chem. Phys.*, **8,** 212 (1940).

Bhatia, S. K., "Analysis of Distributed Pore Closure in Gas-Solid Reactions," *AIChE J.*, **31,** 642 (1985).

Bhatia, S. K., and D. D. Perlmutter, "A Random-Pore Model for Fluid-Solid Reactions. I: Isothermal, Kinetic Control," *AIChE J.*, **26,** 379 (1980).

Borgwardt, R. H. "Kinetics of the Reaction of SO_2 with Calcined Limestone," *Environ. Sci. Technol.*, **4,** 59 (1970).

Broadbent, S. R., and J. M. Hammersley, "Percolation Processes," *Proc. of Cambridge Phil. Soc.*, **53,** 629 (1957).

Costa, E. C., and J. M. Smith, "Kinetics of Noncatalytic, Nonisothermal, Gas-Solid Reactions: Hydrofluorination of Uranium Dioxide," *AIChE J.*, **17,** 947 (1971).

de Boor, C., *A Practical Guide to Splines,* Springer-Verlag, New York (1978).

Feng, C., and W. E. Stewart, "Practical Models for Isothermal Diffusion and Flow of Gases in Porous Solids," *Ind. Eng. Chem. Fundam.*, **21,** 143 (1973).

Fisher, M. E., and J. W. Essam, "Some Cluster Size and Percolation Problems," *J. Math. Phys.*, **2,** 609 (1961).

Gavalas, G. R., "A Random Capillary Model with Application to Char Gasification at Chemically Controlled Rates," *AIChE J.*, **26,** 577 (1980).

Hartman, M., and R. W. Coughlin, "Reaction of Sulfur Dioxide with Limestone and the Influence of Pore Structure," *Ind. Eng. Chem. Process Des. Dev.*, **13,** 248 (1974).

———, "Reaction of Sulfur Dioxide with Limestone and the Grain Model," *AIChE J.*, **22,** 490 (1976).

Jackson, R., *Transport in Porous Catalysts,* Elsevier, Amsterdam (1977).

Larson, R. G., L. E. Scriven, and H. T. Davis, "Percolation Theory of Two-Phase Flow in Porous Media," *Chem. Eng. Sci.*, **36,** 57 (1981).

Shante, V. K. S., and S. Kirkpatrick, "An Introduction to Percolation Theory," *Adv. Physics,* **20,** 325 (1971).

Sotirchos, S. V., "On a Class of Random Pore and Grain Models for Gas-Solid Reactions," *Chem. Eng. Sci.* (1986).

Sotirchos, S. V., and V. N. Burganos, "Diffusion in Pore Networks Effective Medium Theory and Smooth Field Approximation," Submitted to *AIChE J.*, (1986).

Sotirchos, S. V., and H. C. Yu, "Modeling of the Transient Behavior of a Porous Solid Particle Undergoing a Solid Product Formation Reaction," AIChE Ann. Meet. San Francisco (Nov., 1984).

———, "Mathematical Modeling of Gas-Solid Reactions with Solid Product," *Chem. Eng. Sci.*, **40,** 2039 (1985).

Stauffer, D., "Scaling Theory of Percolation Clusters," *Physics Repts.*, **54,** 1 (1979).

Ulerich, N. H., E. P. O'Neill, and D. L. Keairns, "The Influence of Limestone Calcination on the Utilization of the Sulfur-Sorbent in Atmospheric Pressure Fluid-Bed Combustors," EPRI ER-426, Final Report (1977).

Yortsos, Y. C., and M. Sharma, "Application of Percolation Theory to Noncatalytic Gas-Solid Reactions," AIChE Ann. Meet., San Francisco (Nov., 1984).

Yu, H. C., "Theoretical and Experimental Studies on Gas-Solid Reactions with Solid Product," Ph.D. Thesis, Univ. Rochester (1986).

Manuscript received Jan. 23, 1986, and revision received July 11, 1986.